Available online at www.sciencedirect.com

ScienceDirect

Current Opinion in Chemical Biology

Near-infrared fluorescent proteins engineered from bacterial phytochromes

Daria M Shcherbakova[1], Mikhail Baloban[1] and Vladislav V Verkhusha[1,2]

Near-infrared fluorescent proteins (NIR FPs), photoactivatable NIR FPs and NIR reporters of protein–protein interactions developed from bacterial phytochrome photoreceptors (BphPs) have advanced non-invasive deep-tissue imaging. Here we provide a brief guide to the BphP-derived NIR probes with an emphasis on their *in vivo* applications. We describe phenotypes of NIR FPs and their photochemical and intracellular properties. We discuss NIR FP applications for imaging of various cell types, tissues and animal models in basic and translational research. In this discussion, we focus on NIR FPs that efficiently incorporate endogenous biliverdin chromophore and therefore can be used as straightforward as GFP-like proteins. We also overview a usage of NIR FPs in different imaging platforms, from planar epifluorescence to tomographic and photoacoustic technologies.

Addresses
[1] Department of Anatomy and Structural Biology and Gruss-Lipper Biophotonics Center, Albert Einstein College of Medicine, Bronx, NY 10461, USA
[2] Department of Biochemistry and Developmental Biology, Faculty of Medicine, University of Helsinki, Helsinki 00290, Finland

Corresponding author: Verkhusha, Vladislav V (vladislav.verkhusha@einstein.yu.edu)

Current Opinion in Chemical Biology 2015, **27**:52–63

This review comes from a themed issue on **Molecular imaging**

Edited by **Samie Jaffrey** and **Atsushi Miyawaki**

http://dx.doi.org/10.1016/j.cbpa.2015.06.005

Introduction

Near-infrared (NIR) fluorescent probes are superior for deep-tissue and whole-body imaging of small mammals because of reduced autofluorescence, low light scattering and minimal absorbance of hemoglobin, melanin and water in the NIR 'optical window' (~650–900 nm) of mammalian tissue [1]. Significant efforts to develop NIR fluorescent proteins (FPs) from the GFP-like family of proteins resulted in FPs with autocatalytically formed chromophores exhibiting maximally red-shifted absorbance of 611 nm in TagRFP657 [2] and fluorescence of 675 nm in TagRFP675 [3]. The most far-red shifted chromophore found in PSmOrange absorbs at 634 nm and fluoresces at 662 nm [4], however, its formation requires an irradiation with high-power green light. Neither of these protein have both excitation and emission maxima within the NIR optical window (Figure 1a).

To overcome this likely fundamental limit of the chromophore chemistry of the GFP-like FPs [5], recently another family of proteins was employed to engineer truly NIR FPs, namely bacterial phytochrome photoreceptors (BphPs) (Figure 1b). BphPs belong to a large family of the phytochrome photoreceptors found in plants, algae, fungi, bacteria and cyanobacteria, which use linear tetrapyrrole compounds, also known as bilins, as a chromophore [6]. The utility of phytochromes for development of fluorescent probes was first explored a decade ago by Lagarias and co-workers [7]. Among phytochromes, BphPs are the most suitable templates for engineering of NIR FPs. By contrast to plant and cyanobacterial phytochromes, BphPs utilize the most far-red absorbing bilin, biliverdin IXα (BV) [8–10]. Being an enzymatic product of heme degradation (Figure 1c), BV is ubiquitous in many eukaryotic organisms including flies, fishes and mammals, unlike tetrapyrrole chromophores of all other phytochrome types [11]. This important feature makes BphP applications in live mammalian cells, tissues and whole mammals as easy as conventional GFP-like FPs, requiring no enzymes or exogenous cofactors [12].

Recently, numerous BphP-based NIR fluorescent probes of different phenotypes have become available. They consist of permanently fluorescent NIR FPs [13••,14–16,17••,18], photoactivatable NIR FPs [19] and NIR reporters of protein–protein interaction [20•,21–23].

Here we overview available NIR FPs and their applications. We describe NIR FP phenotypes and molecular basis of their fluorescence. We discuss NIR FP characteristics including their advantages and limitations. Next we focus on NIR FP applications in basic biology and biomedicine. We overview imaging modalities beyond planar imaging that allow for higher resolution and sensitivity. Lastly, we provide a brief perspective on future NIR FPs.

Phenotypes and properties of near-infrared fluorescent proteins

In natural BphP photoreceptors, BV isomerizes at its 15/16 double bond upon light absorption [6]. This conformational

change is sensed by a photosensory module and is transmitted to an output effector domain, initiating the light-driven molecular signaling pathway. The photosensory module is formed by PAS (Per-ARNT-Sim repeats), GAF (cGMP phosphodiesterase/adenylate cyclase/FhlA transcriptional activator), and PHY (phytochrome-specific) domains (Figure 1b). BV is located in a pocket of the GAF domain and is covalently attached to a conserved Cys residue in the N-terminal extension of the PAS domain. This N-terminal extension passes through a lasso in the GAF domain, forming a figure-of-eight knot structure [24]. Although the PAS-GAF domains are minimally required for BV binding, the PHY domain is important for the chromophore photoconversion and light-driven signal transduction [25,26]. Two states corresponding to two distinct BV conformations are historically called as Pr ('pigment red absorbing'; 15/16 double bond is in a *cis* conformation) and Pfr ('pigment far-red absorbing'; 15/16 double bond in a *trans* conformation).

The interaction of the BV chromophore with the apoprotein and its photochemistry defines NIR FP characteristics and results in several NIR FP phenotypes. Engineering of BphPs into permanently fluorescent NIR FPs (Figure 1d) requires a stabilization of the Pr state of the BV chromophore to decrease a probability of non-radiative energy dissipation that is achieved by truncation to the PAS-GAF domains and introduction of amino acid substitutions into the chromophore immediate environment [16,17••,18]. In recent years, a number of permanently fluorescent NIR FPs were engineered from different BphPs (Table 1). Majority of these proteins are dimers. Although some NIR FPs behave as monomers in *in vitro* assays, their proper localization in fusion constructs in mammalian cells was not shown. The common feature of all NIR FPs is their relatively low quantum yield comparing to GFP-like FPs. However, the high extinction coefficients and NIR-shifted spectra made them superior probes for *in vivo* imaging.

Fluorescent brightness in mammalian cells (also called effective brightness) is the important parameter for NIR FP applications (Table 1). The effective brightness depends on molecular brightness, intracellular folding and stability, affinity and specificity to BV chromophore, intracellular BV concentration and protein expression level. Low efficiency and specificity of BV binding to the apoprotein substantially decreases the cellular fluorescence because of the competition from other heme-related compounds including protoporphyrins [27,28]. Among NIR FPs, proteins of an infra-Red Fluorescent Protein (iRFP) series have been developed using extensive screening of mutants for fluorescence in mammalian cells [13••,17••]. As a result, iRFPs do not require supply of exogenous BV and can be used by delivering of a single gene to cells. By contrast, NIR FPs of an Infrared Fluorescent Protein (IFP) series require the BV supply [18] or co-expression of heme oxygenase [14], which may affect cell metabolism and proliferation as heme oxygenase is the oxidative stress-inducible enzyme [29,30].

Imaging of several biological processes *in vivo* requires spectrally distinct NIR FPs. By mutating residues in the BV-binding pocket a set of multicolor permanently fluorescent iRFPs has been developed [13••]. Recently, we uncovered a mechanism of the spectral blue-shift in BphP-derived NIR FPs (unpublished data). It was found that the chromophores in blue-shifted NIR FPs differ from the chromophores in red-shifted NIR FPs developed from the same BphP template. In natural BphPs and in red-shifted NIR FPs, the BV chromophore covalently binds to the Cys residue in the PAS domain via $C3^2$ carbon of the side chain of pyrrole ring A (Figure 1d). In blue-shifted NIR FPs, however, BV binds to the Cys residue in the GAF domain, resulting in blue-shifted chromophores linked via either $C3^2$ or $C3^1$ carbon atoms of the side chain of pyrrole ring A (Figure 1d).

By engineering of a whole photosensory module consisting of the PAS-GAF-PHY domains, two photoactivatable NIR FPs (PAiRFPs) were developed from a subtype of BphPs, called bathy BphPs, whose ground state is Pfr [19]. Initially in the dark (non-fluorescent) Pfr state, PAiRFPs photoconvert into the fluorescent Pr state upon illumination with NIR light in the range of ~650–800 nm (Figure 1e). The light-induced conversion from Pr to initial Pfr state is disabled in PAiRFPs, however, a slow thermal conversion results in relaxation back to the dark Pfr state, enabling photoactivation-relaxation cycles.

Domain organization of BphPs is favorable for design of split reporters of protein–protein interactions. Several such reporters have been developed using reconstitution of the PAS and the GAF domains into a fluorescent NIR FP via bimolecular fluorescence complementation [20•,21–23] (Figure 1f, Table 1). Among them, iSplit engineered from iRFP713 exhibits the highest cellular brightness and does not require supply of exogenous BV to mammalian cells and tissues [20•]. The complementation of iSplit reporter is irreversible. Recently, fluorescence of an IFP Protein-fragment Complementation Assay (IFP PCA) reporter was shown to be reversible [21]. Reversibility of IFP PCA complementation is not clearly understood. The knot structure between the N-terminus of the PAS domain with covalently bound BV and the lasso loop of the GAF domain where BV is positioned may inhibit dissociation of the reconstituted NIR FP [24]. Likely, the observed IFP PCA reversibility results from a non-covalently incorporated BV.

Biological applications of near-infrared fluorescent proteins

Advanced NIR FPs are superior probes for non-invasive *in vivo* imaging over GFP-like FPs. Deeper tissue penetration

Figure 1

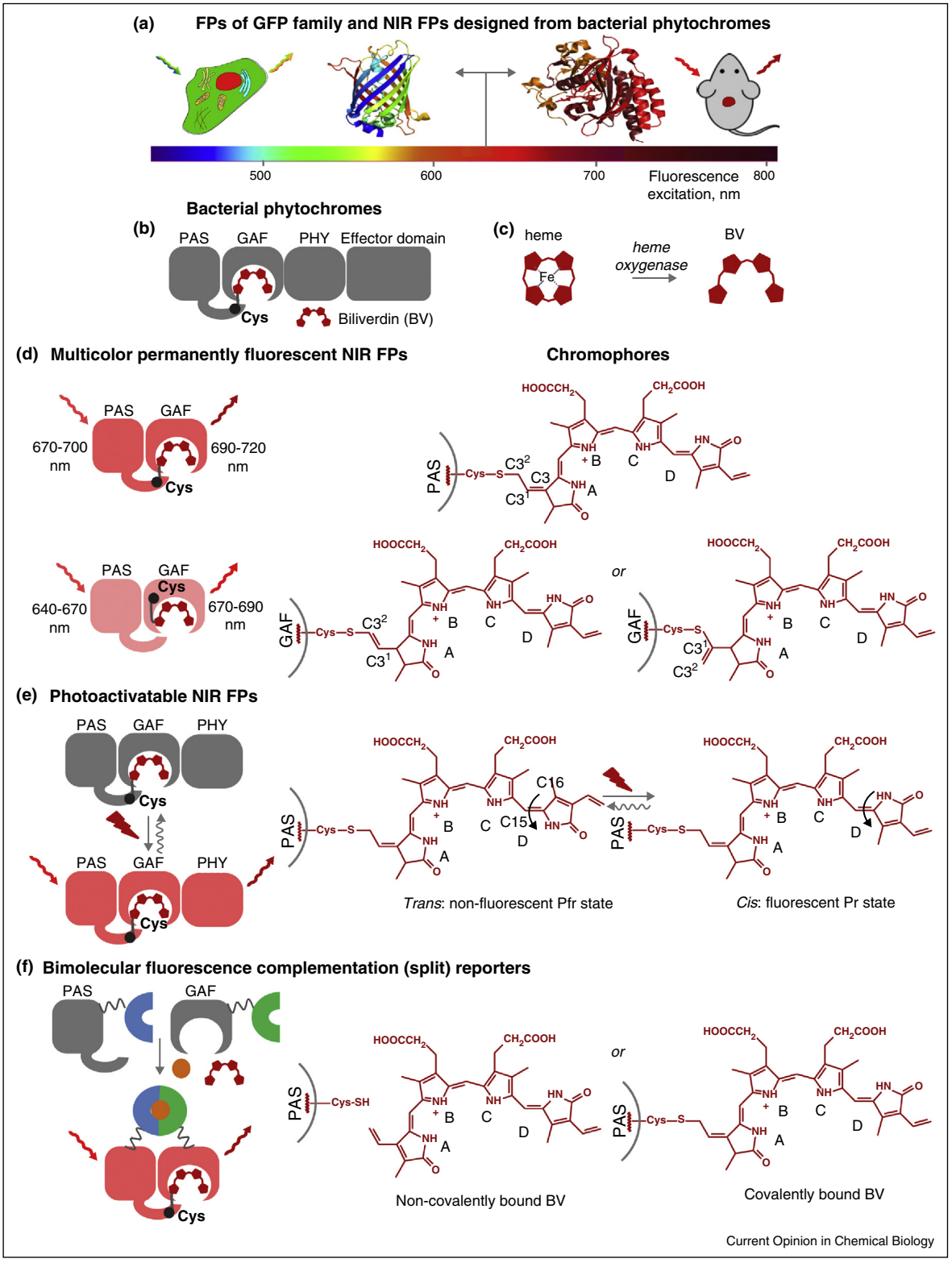

Phenotypes of near-infrared fluorescent proteins (NIR FPs) engineered from bacterial phytochrome photoreceptors (BphPs) and their chromophore photochemistry. **(a)** By contrast to GFP-like FPs, BphP-based NIR FPs have both excitation and emission peaks in the NIR window (650–900 nm) where mammalian tissue is most transparent to light, and scattering and autofluorescence are low. Therefore, NIR FPs are the optimal fluorescent probes for *in vivo* imaging, while bright GFP-like FPs are the good choice for microscopy. **(b)** The domain architecture of BphPs. The

of NIR fluorescence excitation and emission light and lower autofluorescence in the NIR region lead to better signal-to-background ratio of NIR FPs in imaging beyond few millimeters from a surface (Figure 2), as was demonstrated in direct comparison with the most red-shifted GFP-like FPs [13••]. Unlike luciferases, fluorescence of advanced NIR FPs does not depend on exogenous substrates and produce stable signal over time allowing longitudinal imaging.

NIR FPs have been widely applied to cancer studies. Proteins of the iRFP series enabled visualization of small tumors at early stages, monitoring tumor growth and tracking metastases [13••,31•]. In particular, iRFP713 protein performed well as a fluorescent marker in tumors located in deep organs, such as liver and prostate, and intrabone tumors, such as intracranial glioblastoma and intratibial osteosarcoma (Figure 2a) [32]. Using various imaging modalities (Figure 3) iRFP713 enabled imaging progression of inflammatory breast cancer and its metastases in lymph nodes [33] and detection metastatic targets of melanoma in whole body (Figure 3b) [32]. iRFP713 also allowed to monitor tumor growth and metastases in an orthotopic prostate cancer model (Figure 3f) [31•,34]. Single circulating metastatic cells labeled with iRFP713 were detected in blood vessels of a mouse [35]. NIR FPs hold a great potential for preclinical testing of anti-cancer drugs as they can be used to visualize tumor relapse and regression following the medical treatment [36].

The ability to image labeled cell populations in a whole animal makes NIR FPs useful for stem cell studies. For example, iRFP713 allowed to non-invasively track the transplanted cardiac progenitor cells in the ischemic mouse hearts *in vivo* (Figure 2b) [37]. Moreover, the transplanted iRFP713 bone marrow cells were able to reconstitute the hematopoietic system of the irradiated mice, indicating the reconstitution capacity of stem cells expressing iRFP713 [38•].

Applicability of NIR FPs is not limited to particular cell types or organs. All iRFPs are non-cytotoxic stable proteins [13••]. Recently, iRFP713 transgenic mice have been developed (Figure 2c) [38•]. The mice were healthy as judged from serum and blood cell indices and produced healthy offspring. iRFP713 fluorescence was ubiquitously detected in all tissues including brain, heart, liver, kidney, spleen, lung, pancreas, bone, testis, thymus and adipose tissues.

Advanced NIR FPs find their use in neuroscience for imaging of neuronal cells and detection of their metabolic processes. For example, iRFP713 was expressed in primary culture of hippocampal neurons (Figure 2d) and in retinal neurons in a mouse [39]. NIR FPs are particularly useful for studies related to retinal neurons because NIR excitation light does not damage photoresponsiveness of retina unlike visible light required for GFP-like FPs.

The ability to efficiently utilize endogenous BV present in protozoan parasites allows testing of new drugs in preclinical parasitic disease studies *ex vivo* and *in vivo*. Recently, the phenotypic high-throughput screening of drug collections against *Leishmania* species expressing iRFP713 was performed. Moreover, the NIR fluorescent *Leishmania* parasites were used to monitor the development of the *in vivo* infection by imaging mice for 20 weeks [40].

Spectrally distinct NIR FPs enable labelling of several tissues and organs *in vivo*. The most blue-shifted iRFP670 and red-shifted iRFP713 or iRFP720 are well resolved using two filter sets either in epifluorescence microscopy or in whole-body imaging (Figure 2e) [13••]. Two iRFPs allowed simultaneous visualization of a liver and a tumor or two closely located tumors in living mice. The number of NIR FPs can be increased up to five with the use of linear spectral unmixing algorithms available in modern confocal microscopes and whole-body imaging platforms (Figure 2f).

NIR FPs of the iRFP series are also used in microscopy as additional fluorescent colors, resulting in imaging of multiple FP fusions in a single cell [41,42].

Photoactivatable PAiRFPs allowed increasing of imaging sensitivity under highly autofluorescent conditions. Autofluorescence background can be removed by subtracting the images made before and after photoactivation (Figure 2g). PAiRFPs were also applied for photolabelling and short-term noninvasive tracking in animals, as

(Figure 1 Legend Continued) photosensory module of BphPs consists of the PAS, GAF and PHY domains. Light irradiation activates the photosensory module, which then transmits the signal to the effector domain to initiate a molecular signaling pathway. As a chromophore, BphPs use biliverdin (BV), which is located in a pocket of the GAF domain and is covalently bound to the Cys in the PAS domain. **(c)** In eukaryotic cells BV is produced from heme by heme oxygenase. **(d)** Multicolor permanently fluorescent FPs differ in the way they bind the BV chromophore. The red-shifted NIR FPs (top) bind it the same way as natural BphPs, that is, by the Cys in the PAS domain via $C3^2$ carbon atom of the pyrrole ring A. The engineered blue-shifted NIR FPs (bottom) bind BV by the Cys in the GAF domain via either $C3^2$ or $C3^1$ carbon atoms of side chain of the ring A. In the resulting chromophore adducts, one double bond in the ring A is removed from the conjugation with the rest of the π-electron system resulting in the spectral blue shift. **(e)** Photoactivatable NIR FPs consist of a whole photosensory module and, similarly to natural BphPs, the bound BV undergoes the *cis-trans* isomerization of the C15/C16 double bond. By contrast to natural BphPs, the light-induced transition from the fluorescent Pr to non-fluorescent Pfr state is blocked and slowly occurs in darkness only. **(f)** The bimolecular fluorescence complementation (split) reporters are based on the reconstitution of a fluorescent NIR FP molecule in response to physical interaction of a pair of the fused protein partners. In the process of NIR FP reconstitution, BV chromophore enters the pocket of the GAF domain and may remain non-covalently bound or may form a covalent bond with the Cys in the PAS domain.

Table 1

Properties of near-infrared fluorescent proteins and reporters engineered from bacterial phytochromes

Fluorescent protein	Bacterial phytochrome template	Excitation, nm, emission, nm	Extinction coefficient, M^{-1} cm^{-1}	Quantum yield, %	Molecular weight and oligomeric state	Brightness in mammalian cells relative to iRFP713, % [b]	Demonstrated applications in cells and animals	Specific properties related to applications	Reference
Permanently fluorescent proteins									
IFP1.4	*Dr*BphP	684, 708	92 000 (102 000)[a]	7.7 (7.0)[a]	35 kDa, monomeric[c]	8 (increased to 14 after 2 h incubation with 25 μM BV)	Whole-body imaging of liver	Supply of exogenous BV chromophore or co-expression of heme oxygenase is required	[18]
Wi-Phy	*Dr*BphP	700, 722	118 000	6.3	35 kDa, monomeric[c]	ND	ND		[16]
IFP2.0	*Dr*BphP	690, 711	86 100	8.0	35 kDa, dimeric[d]	8 (without supply of exogenous BV) [d] ~100 (with co-expressed heme oxygenase)	Whole-body imaging of tumors, imaging of tissues in *Drosophila* larva		[14]
IFP1.4rev	*Dr*BphP	685, 708	131 500	8.7	35 kDa, monomeric[c]	ND	ND		[15]
iRFP670	*Rp*BphP6	643, 670	114 000	11.1	35 kDa, dimeric	119	Multicolor microscopy and whole-body imaging, photoacoustic tomography, fluorescence lifetime imaging, tumors and metastases in various tissues, stem cells, transgenic mice	Efficient binding of endogenous BV chromophore in many mammalian cell types. No need for supply of exogenous BV or co-expression of heme oxygenase	[13••,17••]
iRFP682	*Rp*BphP2	663, 682	90 000	11.3		105			
iRFP702	*Rp*BphP6	673, 702	93 000	8.2		61			
iRFP713	*Rp*BphP2	690, 713	98 000	6.3		100			
iRFP720	*Rp*BphP2	702, 720	96 000	6.0		110			
Photoactivatable fluorescent proteins									
PAiRFP1	*At*BphP2	690[e], 717[e]	67 100	4.8	57 kDa, dimeric	25 (increased to 43 after 2 h with 25 μM BV)	Whole-body imaging with enhanced signal-to-background ratio in autofluorescent tissues	Photoactivatable by both far-red and NIR light. Half-time of thermal relaxation to dark state is ~1 h	[19]
PAiRFP2	*At*BphP2	692[e], 719[e]	63 600	4.7		7 (increased to 9 after 2 h with 25 μM BV)		Photoactivatable by both far-red and NIR light. Half-time of thermal relaxation to dark state is ~4 h	

Reporter	Fluorescent protein used in design (excitation, nm, emission, nm)	Extinction coefficient, M^{-1} cm^{-1}	Quantum yield, %	Contrast in cultured mammalian cells, fold	Interacting pairs tested	Advantages	Limitations	Reference
Reporters for protein–protein interaction								
iSplit	iRFP713 (690, 713)	85 500	6.8	>20–50 (~18 in mice)	E-coil and K-coil peptides, FRB and FKBP proteins	High brightness and large complementation contrast. Applicable for *in vivo* protein–protein interaction studies	Irreversible	[20•]
iRFP BiFC system		ND	ND	~5–6 (same in mice)	bJun and bFos, HIV-1 integrase and LEDGF/p75 growth factor	Demonstrated use for drug evaluation in cells. Applicable for *in vivo* protein–protein interaction studies	Irreversible. Lower BiFC contrast than for iSplit. Brightness has not been compared with parental NIR FP	[23]
IFP PCA	IFP1.4 (684, 708)	42 890	6.2	~2 (~20–50 in yeast)	Protein kinase PKA subunits, SHC and GRB2, some known PPIs in yeast	Reversibility. Suitable for imaging of spatiotemporal dynamics of protein–protein interactions	Low brightness and complementation contrast in mammalian cells. Requires supply of exogenous BV or overexpression of heme oxygenase.	[21]
Fragmented IFP		ND	ND	ND (up to 22 in bacteria)	IAAL-E3 and IAAL-K3 peptides, CheA and CheY proteins	Several fragmented variants developed with different complementation contrast in bacteria	Not tested in mammalian cells. Requires supply of exogenous BV	[22]

[a] Measured in [17••].
[b] Determined as effective NIR fluorescence in HeLa cells with no supply of exogenous BV and after normalization to fluorescence of co-transfected EGFP. Note that the values of brightness may vary in different cell types due to variations in endogenous BV concentration and protein expression level.
[c] Monomeric state was shown by size exclusion chromatography only.
[d] Our size exclusion chromatography (SEC) and HeLa cell expression data. For SEC, the HiLoad 16/600 Superdex 200 column and the 10 mM Hepes buffer pH 7.4 containing 50 μM EDTA, 10% glycerol, 150 mM NaCl, 1 mM DTT, 0.2 mM PMSF, 0.01% EP-40 and 0.2 mM benzodiazepine were used.
[e] Corresponds to a photoactivated state. BV, biliverdin. PPI, protein–protein interaction. ND, not determined.

Figure 2

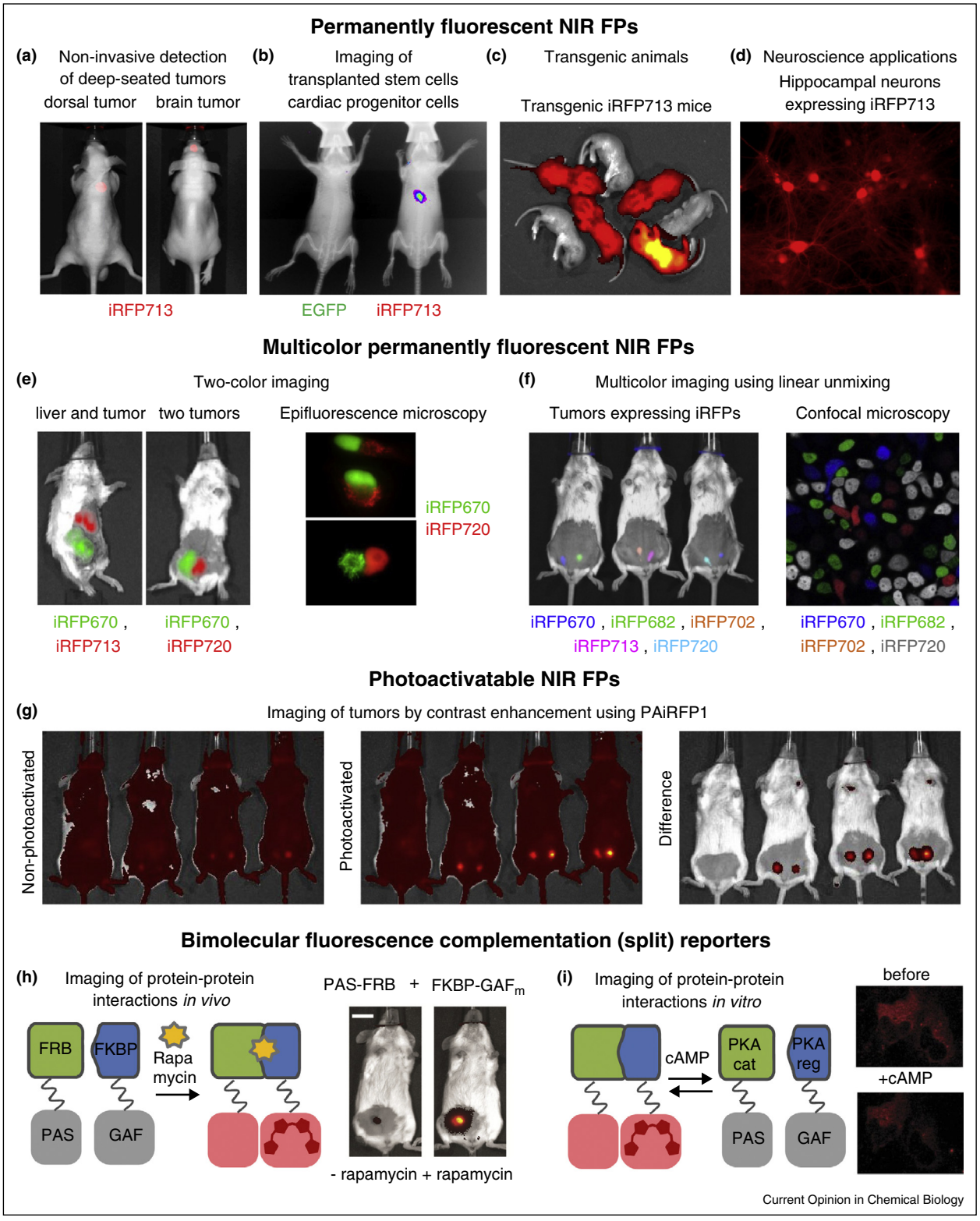

Applications of NIR FPs as probes for fluorescence microscopy and whole-body imaging. **(a)** Whole-body imaging of a dorsal tumor obtained as a metastasis lesion after tail vein injection of iRFP713-labeled IGR-37 melanoma cells (left), and a brain tumor derived by intracranial injection of iRFP713-labeled U87 MG glioblastoma cells (right). Adapted from [32]. Copyright 2014 Society of Photo Optical Instrumentation Engineers. **(b)** Whole-body imaging of cardiac progenitor cells labeled with either EGFP (left mouse) or iRFP713 (right mouse) transplanted to the heart after

they can be photoactivated in a spatially selective manner [19].

The NIR reporter iSplit enabled visualization of model protein–protein interactions in cultured cells and living animals (Figure 2h). Although the reporter is irreversible, detection of infrequent repetitive binding events was possible due to the relatively fast degradation of the complemented iSplit complex *in vivo*. The IFP PCA split reporter is likely suboptimal for *in vivo* imaging because of the ~10-fold lower brightness than iSplit and strong requirement of exogenous BV. Nevertheless, its reversibility allowed the spatiotemporal localization of several protein–protein interactions in yeast and mammalian cells (Figure 2i).

Near-infrared fluorescent proteins in advanced imaging technologies

NIR FPs enable multiple *in vivo* imaging modalities, from simple techniques suitable for high throughput workflow to advanced methods of 3D reconstruction, sub-millimeter spatial resolution and precise data quantification.

Planar fluorescence imaging is the most widely used method for NIR FP visualization, because it is technically simple and inexpensive (Figure 3a,b). Major limitation of this technique is that the surface-measured fluorescence cannot be unambiguously assigned to 3D distribution of fluorescent objects inside the specimen.

Unlike planar imaging, a tomography technique can retrieve 3D imaging data. In fluorescence molecular tomography (FMT), a wide-field illumination is replaced with sequential scans of focal light sources [43,44]. Through imaging of multiple source-detector pairs and application of a model of light propagation in the tissue, a 3D image can be reconstructed. Current platforms for planar imaging can also perform fluorescence diffuse tomography by acquiring several images with scanning excitation source in a trans-illumination mode with subsequent reconstruction (Figure 3c,d). Although less precise than specialized systems, diffuse tomography allowed 3D localization of a tumor and a liver labeled with distinct iRFPs [13••].

For better spatial resolution, an acquisition of multiple 2D projections is required. This can be achieved by using either the multiple source-detector pairs, a scanning excitation source or a rotary gantry-based system [31•] (Figure 3e). Furthermore, a combination of fluorescence tomography with anatomical imaging modalities, such as a magnetic resonance imaging (MRI) and an X-ray computed tomography (XCT), provides additional information. Anatomical data obtained in XCT can be used for more precise image reconstitution by accounting for tissue interfaces and for absorption and scattering properties within each tissue type. Using iRFP713, tomographic imaging of an orthotopic prostate cancer was demonstrated (Figure 3f). The fluorescence signal has been co-registered with a positron emission tomography (PET) and XCT [31•]. Moreover, a brain glioma tumor expressing iRFP713 was reconstructed using a hybrid FMT-XCT imaging (Figure 3g) [45•].

Measurement of parameters other than fluorescence intensity, such as fluorescence lifetime or absorption, provides additional data for image reconstruction. Fluorescence lifetime imaging using time-domain (TD) detection allows signal separation from tissue autofluorescence on the basis of the characteristic fluorescence lifetimes. The TD setup requires ~10^{-11}–10^{-10} s pulses for

(Figure 2 Legend Continued) myocardial infarction. The fluorescence images are overlaid with the X-ray images Adapted from [37]. Copyright 2014 (available under a Creative Commons Attribution license). **(c)** Advanced NIR FPs are non-cytotoxic and well expressed in all tissues. The image shows newborn iRFP713-transgenic mice and wild-type non-fluorescent littermates. Adapted from [38•]. Copyright 2014 by the Japanese Association for Laboratory Animal Science. **(d)** Microscopy image showing that iRFP713 is ubiquitously expressed in the primary culture of mouse hippocampal neurons infected with iRFP713-encoded lentivirus. **(e)** Two-color image of a mammary gland tumor derived from iRFP670-labeled MTLn3 cells and a liver expressing iRFP713 after infection with iRFP713-encoding adenovirus (left mouse). Two-color image of two MTLn3 tumors, one expressing iRFP670 and another iRFP720 (right mouse). Two-color epifluorescence microscopy of HeLa cells transiently co-expressing iRFP670 and iRFP720 targeted to nucleus and mitochondria. The fluorescence signals in all images are presented in pseudocolors. Adapted from [13••]. **(f)** Multicolor *in vivo* imaging of five types of MTLn3-derived tumors expressing different iRFPs in mice (left). The 19 images in different spectral channels were obtained and used for linear spectral unmixing. Multicolor imaging of MTLn3 cells expressing iRFP670, iRFP682, iRFP702 and iRFP720 obtained using confocal microscopy with spectral detection and subsequent linear unmixing (right). The fluorescence signals in all images are presented in pseudocolors. Adapted from [13••]. **(g)** Photoactivatable NIR FPs allow to increase imaging sensitivity. The contrast enhancement is achieved by acquiring two images: before (left) and after (middle) photoactivation. By subtracting the former image from the latter one the contribution from autofluorescence is largely decreased (right). The tumors were derived from PAiRFP1-expressing MTLn3 cells. Adapted from [19]. **(h)** Schematics of the rapamycin induced interaction of FKBP and FRB proteins studied with iSplit reporter (left). Without rapamycin, non-interacting fusion proteins do not cause complementation of a NIR FP. After addition of rapamycin, FKBP and FRB interact with each other and bring the fused PAS and GAF domains in a close proximity required for reconstitution of NIR fluorescence. GAFm denotes a mutated version of the GAF domain from iRFP713 optimized for the complementation in the iSplit reporter. *In vivo* imaging of rapamycin-induced protein–protein interaction in MTln3-based tumor co-expressing PAS-FRB and FKBP-GAFm fusion proteins (right). Adapted from [20•]. **(i)** Schematics of cAMP-induced dissociation of two protein kinase A (PKA) subunits studied with IFP PCA reporter (left). Initially reconstituted IFP PCA is fluorescent, because the PAS and GAF domains are fused to interacting catalytic subunit α and regulatory subunit IIβ. Signaling from β_2-adrenergic receptor induces an increase in cAMP concentration and dissociation of two subunits of PKA, which can be detected by a decrease in NIR fluorescence. Microscopy images of U2OS cells co-expressing two constructs are shown before and after activation of β_2-adrenergic receptor causing cAMP increase (right). Adapted from [21], with permission from Nature Publishing Group.

Figure 3

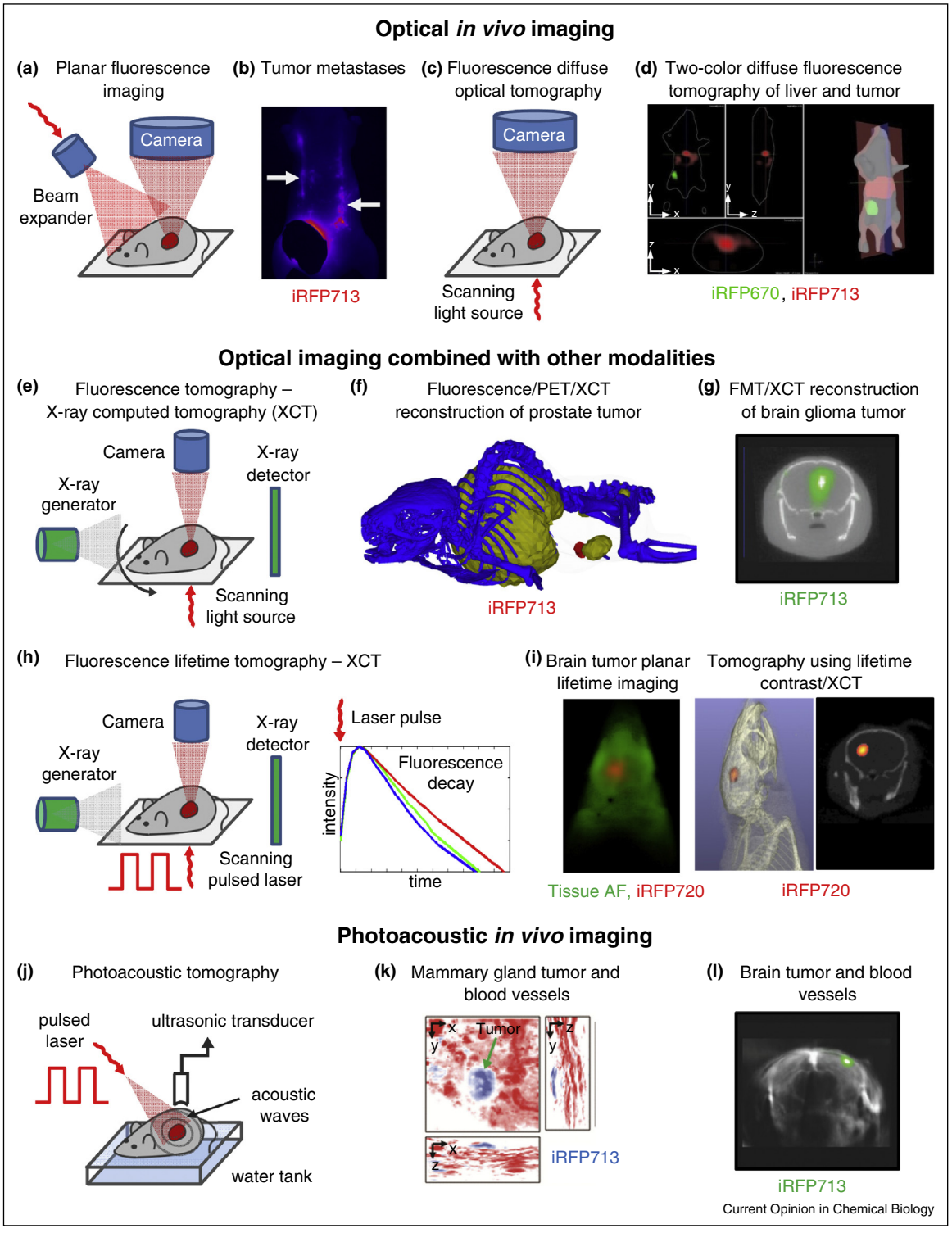

Detection of NIR FPs using different *in vivo* imaging techniques. **(a)** Schematics of planar fluorescence imaging setup that involves wide-field excitation and detection of emission light from a specimen. **(b)** Visualization of metastasis in mice as an example of planar fluorescence imaging. The metastasis in lymphatic channels (indicated by arrows) originate from a mammary gland tumor (covered) formed after implantation of iRFP713-labeled MDA-MB-231 cells. (Courtesy of E.M. Sevick-Muraca, University of Texas, TX). **(c)** Schematics of fluorescence diffuse tomography setup. The scanning light source in transillumination mode allows to obtain a series of 2D images used for reconstruction. **(d)** 3D two-color visualization of a tumor derived from iRFP670-labeled MTLn3 cells and a liver expressing iRFP713. Adapted from [13••]. **(e)** Schematics of a fluorescence tomography combined with X-ray computed tomography (XCT). Acquisition of multiple 2D projections is possible by using either

detection of fluorescence decay (Figure 3h). The rejection of tissue autofluorescence substantially increases the detection sensitivity. This approach allowed visualization of $\sim 5 \times 10^4$ iRFP720-labeled cancer cells in mouse lungs [46•]. Tomographic implementation of fluorescence lifetime detection, such as asymptotic fluorescence lifetime tomography-XCT imaging, uses anatomical information obtained in XCT for better reconstruction. Using fluorescence lifetime tomography, the 3D distribution of iRFP720-labeled cells in deep-seated organs, such as lungs and brain, was demonstrated (Figure 3i) [46•].

The main reason for a limited spatial resolution of NIR fluorescence imaging is the tissue light scattering. Photoacoustic tomography allows a submillimeter resolution at depths of several millimeters inside tissue [47]. In photoacoustic imaging, a specimen is illuminated with $\sim 10^6$–10^7 Hz pulsed laser. The thermoelastically induced ultrasonic waves resulted from light absorption by spatially localized chromophores are detected (Figure 3j). The higher spatial resolution results from much lower scattering of ultrasonic waves in tissue. In addition to labeled cells, photoacoustic tomography allows detection of endogenous absorbing biomolecules, such as hemoglobin in blood. The usage of NIR FPs of the iRFP series as efficient photoacoustic probes was demonstrated in several studies [45•,48•,49,50] including photoacoustic tomography of mammary gland tumor with surrounding blood vessels (Figure 3k) [48•].

Several *in vivo* imaging modalities were recently compared side by side [45•]. The deep-seated glioma tumor was detected using the planar epi-illumination and trans-illumination setups, a hybrid FMT-XCT system and a photoacoustic tomography, such as multispectral optoacoustic tomography (MSOT). The expressed iRFP713 allowed to visualize the tumor using all methods, however, with different resolution. Planar fluorescence imaging provided the lowest resolution that largely depended on the depth of the tumor, FMT-XCT resulted in ~1 mm resolution and MSOT achieved ~0.1 mm resolution with the comparable sensitivity (Figure 1l) [45•].

Conclusions

NIR FPs engineered from bacterial phytochromes have a great potential as the genetically encoded probes for non-invasive *in vivo* imaging in biological and pre-clinical studies. Molecular engineering of future brighter NIR FPs, which do not require exogenous supply of BV chromophore, together with the ongoing developments in optical imaging technologies will advance basic and translational studies utilizing small animals. Furthermore, a design of truly monomeric NIR FPs, which effectively and specifically incorporate intracellular BV, should allow tagging of protein molecules for visualization of their behavior at the tissue and whole-body levels. Importantly, multicolor monomeric NIR FPs fused to specific protein domains will be utilized as reporters and biosensors of biological processes *in vivo*.

Acknowledgments

We thank Yoshihiro Miwa (University of Tsukuba, Japan), Eva M. Sevick-Muraca (University of Texas, TX), Yaoliang Tang (Georgia Regents University, GA) and Assou El-Battari (Aix-Marseille University, France) for sharing their images of the iRFP713-expressing mouse models. This work was supported by the grants GM073913, GM108579 and CA164468 from the US National Institutes of Health and ERC-2013-ADG-340233 from the EU FP7 program.

References and recommended reading

Papers of particular interest, published within the period of review, have been highlighted as:

- • of special interest
- •• of outstanding interest

1. Weissleder R: **A clearer vision for in vivo imaging**. *Nat Biotechnol* 2001, **19**:316-317.

2. Morozova KS, Piatkevich KD, Gould TJ *et al.*: **Far-red fluorescent protein excitable with red lasers for flow cytometry and superresolution STED nanoscopy**. *Biophys J* 2010, **99**:L13-L15.

3. Piatkevich KD, Malashkevich VN, Morozova KS *et al.*: **Extended Stokes shift in fluorescent proteins: chromophore-protein interactions in a near-infrared TagRFP675 variant**. *Sci Rep* 2013, **3**:1847.

(Figure 3 Legend Continued) multiple source-detector pairs, a scanning excitation source or a rotary gantry-based system. Co-registration of X-ray computed tomography (XCT) provides anatomical information and is used for more precise tomographic reconstruction of the fluorescence signal. **(f)** Hybrid fluorescence/Positron Emission Tomography (PET)/XCT imaging of a prostate tumor derived from iRFP713-expressing PC3 prostate cancer cells. XCT signal is in blue (bones), PET signal is in yellow (liver, prostate and bladder) and iRFP713 signal (tumor) is in red. Adapted from [31•]. Copyright 2014 Society of Photo Optical Instrumentation Engineers. **(g)** Hybrid fluorescence molecular tomography (FMT)/XCT imaging of a mouse brain tumor derived from iRFP713-expressing glioblastoma U87 cells. Adapted from [45•]. Copyright 2014 Springer group. **(h)** Schematics of a fluorescence tomography with a lifetime contrast combined with XCT. For detection of the fluorescence decay curves (right), fluorescence lifetime imaging with the time-domain (TD) detection uses an ultrafast scanning laser (left). This technique allows to separate autofluorescence from NIR FP signal on the basis of their characteristic fluorescence lifetimes. **(i)** Tomography with fluorescence lifetime contrast of a brain tumor derived from iRFP720-expressing MTLn3 cells. (left) Planar image showing an overlay of the unmixed signals from autofluorescence (green) and iRFP720 (red). (middle and right) The tomographic reconstruction of a tumor co-registered with XCT. Adapted from [46•]. **(j)** Schematics of a photoacoustic (also called optoacoustic) tomography. An animal is illuminated with a pulsed laser that induces the thermoelastic expansion of the localized absorbing objects. This expansion generates ultrasonic waves, which are detected. In addition to NIR FPs, the photoacoustic tomography allows to visualize natural absorbers, such as hemoglobin in blood. **(k)** Photoacoustic imaging of a mammary gland tumor derived from iRFP713-expressing MTLn3 cells (blue) surrounded by blood vessels (red). The image shows an overlay of the spectrally unmixed signals of iRFP713 and total hemoglobin in blood. Adapted from [48•]. **(l)** Photoacoustic imaging of a brain glioblastoma tumor (green) derived from iRFP713-labeled glioblastoma U87 MG cells. The image shows an overlay of a spectrally unmixed signal of iRFP713 and an anatomical image of the head obtained by detection of total hemoglobin in blood. Adapted from [45•]. Copyright 2014 Springer group.

4. Subach OM, Patterson GH, Ting LM *et al.*: **A photoswitchable orange-to-far-red fluorescent protein, PSmOrange**. *Nat Methods* 2011, **8**:771-777.

5. Shcherbakova DM, Verkhusha VV: **Chromophore chemistry of fluorescent proteins controlled by light**. *Curr Opin Chem Biol* 2014, **20**:60-68.

6. Rockwell NC, Lagarias JC: **A brief history of phytochromes**. *Chemphyschem* 2010, **11**:1172-1180.

7. Fischer AJ, Lagarias JC: **Harnessing phytochrome's glowing potential**. *Proc Natl Acad Sci U S A* 2004, **101**:17334-17339.

8. Giraud E, Vermeglio A: **Bacteriophytochromes in anoxygenic photosynthetic bacteria**. *Photosynth Res* 2008, **97**:141-153.

9. Karniol B, Wagner JR, Walker JM, Vierstra RD: **Phylogenetic analysis of the phytochrome superfamily reveals distinct microbial subfamilies of photoreceptors**. *Biochem J* 2005, **392**:103-116.

10. Auldridge ME, Forest KT: **Bacterial phytochromes: more than meets the light**. *Crit Rev Biochem Mol Biol* 2011, **46**:67-88.

11. Kapitulnik J, Maines MD: **The role of bile pigments in health and disease: effects on cell signaling, cytotoxicity, and cytoprotection**. *Front Pharmacol* 2012, **3**:136.

12. Piatkevich KD, Subach FV, Verkhusha VV: **Engineering of bacterial phytochromes for near-infrared imaging, sensing, and light-control in mammals**. *Chem Soc Rev* 2013, **42**:3441-3452.

13. •• Shcherbakova DM, Verkhusha VV: **Near-infrared fluorescent proteins for multicolor in vivo imaging**. *Nat Methods* 2013, **10**:751-754.

Paper reports a set of spectrally distinct iRFPs that enable multicolor imaging in living mice.

14. Yu D, Gustafson WC, Han C *et al.*: **An improved monomeric infrared fluorescent protein for neuronal and tumour brain imaging**. *Nat Commun* 2014, **5**:3626.

15. Bhattacharya S, Auldridge ME, Lehtivuori H *et al.*: **Origins of fluorescence in evolved bacteriophytochromes**. *J Biol Chem* 2014, **289**:32144-32152.

16. Auldridge ME, Satyshur KA, Anstrom DM, Forest KT: **Structure-guided engineering enhances a phytochrome-based infrared fluorescent protein**. *J Biol Chem* 2012, **287**:7000-7009.

17. •• Filonov GS, Piatkevich KD, Ting LM *et al.*: **Bright and stable near-infrared fluorescent protein for in vivo imaging**. *Nat Biotechnol* 2011, **29**:757-761.

Paper reports the first NIR FPs that efficiently incorporates endogenous biliverdin chromophore in mammalian cells and does not require its exogenous supply.

18. Shu X, Royant A, Lin MZ *et al.*: **Mammalian expression of infrared fluorescent proteins engineered from a bacterial phytochrome**. *Science* 2009, **324**:804-807.

19. Piatkevich KD, Subach FV, Verkhusha VV: **Far-red light photoactivatable near-infrared fluorescent proteins engineered from a bacterial phytochrome**. *Nat Commun* 2013, **4**:2153.

20. • Filonov GS, Verkhusha VV: **A near-infrared BiFC reporter for in vivo imaging of protein–protein interactions**. *Chem Biol* 2013, **20**:1078-1086.

Paper reports the first bimolecular fluorescence complementation (split) reporter iSplit engineered from a NIR FP and demonstrates its use for visualization of protein–protein interactions in living mice.

21. Tchekanda E, Sivanesan D, Michnick SW: **An infrared reporter to detect spatiotemporal dynamics of protein–protein interactions**. *Nat Methods* 2014, **11**:641-644.

22. Pandey N, Nobles CL, Zechiedrich L *et al.*: **Combining random gene fission and rational gene fusion to discover near-infrared fluorescent protein fragments that report on protein–protein interactions**. *ACS Synth Biol* 2015, **4**:615-624.

23. Chen M, Li W, Zhang Z *et al.*: **Novel near-infrared BiFC systems from a bacterial phytochrome for imaging protein interactions and drug evaluation under physiological conditions**. *Biomaterials* 2015, **48**:97-107.

24. Stepanenko OV, Bublikov GS, Shcherbakova DM *et al.*: **A knot in the protein structure — probing the near-infrared fluorescent protein iRFP designed from a bacterial phytochrome**. *FEBS J* 2014, **281**:2284-2298.

25. Yang X, Kuk J, Moffat K: **Crystal structure of *Pseudomonas aeruginosa* bacteriophytochrome: photoconversion and signal transduction**. *Proc Natl Acad Sci U S A* 2008, **105**:14715-14720.

26. Takala H, Bjorling A, Berntsson O *et al.*: **Signal amplification and transduction in phytochrome photosensors**. *Nature* 2014, **509**:245-248.

27. Wagner JR, Zhang J, von Stetten D *et al.*: **Mutational analysis of *Deinococcus radiodurans* bacteriophytochrome reveals key amino acids necessary for the photochromicity and proton exchange cycle of phytochromes**. *J Biol Chem* 2008, **283**:12212-12226.

28. Lehtivuori H, Rissanen I, Takala H *et al.*: **Fluorescence properties of the chromophore-binding domain of bacteriophytochrome from *Deinococcus radiodurans***. *J Phys Chem B* 2013, **117**:11049-11057.

29. Bansal S, Biswas G, Avadhani NG: **Mitochondria-targeted heme oxygenase-1 induces oxidative stress and mitochondrial dysfunction in macrophages, kidney fibroblasts and in chronic alcohol hepatotoxicity**. *Redox Biol* 2014, **2**:273-283.

30. Jozkowicz A, Was H, Dulak J: **Heme oxygenase-1 in tumors: is it a false friend?** *Antioxid Redox Signal* 2007, **9**:2099-2117.

31. • Lu Y, Darne CD, Tan IC *et al.*: **In vivo imaging of orthotopic prostate cancer with far-red gene reporter fluorescence tomography and in vivo and ex vivo validation**. *J Biomed Opt* 2013, **18**:101305.

Paper reports a use of iRFP713 in a hybrid fluorescence tomography/positron emission tomography (PET)/X-ray computed tomography (XCT) imaging setup to visualize prostate tumor in living animals.

32. Jiguet-Jiglaire C, Cayol M, Mathieu S *et al.*: **Noninvasive near-infrared fluorescent protein-based imaging of tumor progression and metastases in deep organs and intraosseous tissues**. *J Biomed Opt* 2014, **19**:16019.

33. Agollah GD, Wu G, Sevick-Muraca EM, Kwon S: **In vivo lymphatic imaging of a human inflammatory breast cancer model**. *J Cancer* 2014, **5**:774-783.

34. Zhu BH, Wu G, Robinson H *et al.*: **Tumor margin detection using quantitative NIRF molecular imaging targeting EpCAM validated by far red gene reporter iRFP**. *Mol Imaging Biol* 2013, **15**:560-568.

35. Nedosekin DA, Sarimollaoglu M, Galanzha EI *et al.*: **Synergy of photoacoustic and fluorescence flow cytometry of circulating cells with negative and positive contrasts**. *J Biophotonics* 2013, **6**:425-434.

36. Condeelis J, Weissleder R: **In vivo imaging in cancer**. *Cold Spring Harbor Perspect Biol* 2010, **2**:a003848.

37. Wang Y, Zhou M, Wang X *et al.*: **Assessing in vitro stem-cell function and tracking engraftment of stem cells in ischaemic hearts by using novel iRFP gene labelling**. *J Cell Mol Med* 2014, **18**:1889-1894.

38. • Tran MT, Tanaka J, Hamada M *et al.*: **In vivo image analysis using iRFP transgenic mice**. *Exp Anim/Jap Assoc Lab Anim Sci* 2014, **63**:311-319.

The first report on the development of the iRFP713 transgenic mice. The mice are healthy and express iRFP173 ubiquitously in the body.

39. Fyk-Kolodziej B, Hellmer CB, Ichinose T: **Marking cells with infrared fluorescent proteins to preserve photoresponsiveness in the retina**. *BioTechniques* 2014, **57**:245-253.

40. Calvo-Alvarez E, Stamatakis K, Punzon C *et al.*: **Infrared fluorescent imaging as a potent tool for in vitro, ex vivo and in vivo models of visceral leishmaniasis**. *PLoS Negl Trop Dis* 2015, **9**:e0003666.

41. Kuhar R, Gwiazda KS, Humbert O *et al.*: **Novel fluorescent genome editing reporters for monitoring DNA repair pathway utilization at endonuclease-induced breaks**. *Nucleic Acids Res* 2014, **42**:e4.

42. Sanders TA, Llagostera E, Barna M: **Specialized filopodia direct long-range transport of SHH during vertebrate tissue patterning**. *Nature* 2013, **497**:628-632.

43. Stuker F, Ripoll J, Rudin M: **Fluorescence molecular tomography: principles and potential for pharmaceutical research**. *Pharmaceutics* 2011, **3**:229-274.

44. James ML, Gambhir SS: **A molecular imaging primer: modalities, imaging agents, and applications**. *Physiol Rev* 2012, **92**:897-965.

45. • Deliolanis NC, Ale A, Morscher S *et al.*: **Deep-tissue reporter-gene imaging with fluorescence and optoacoustic tomography: a performance overview**. *Mol Imaging Biol* 2014, **16**:652-660.
Paper compares different imaging technologies side by side, from planar epifluorescence to photoacoustic tomography, using the same mice with brain tumor expressing iRFP713.

46. • Rice WL, Shcherbakova DM, Verkhusha VV, Kumar AT: **In vivo tomographic imaging of deep-seated cancer using fluorescence lifetime contrast**. *Cancer Res* 2015, **75**:1236-1243.
Paper reports the first application of several spectrally distinct iRFPs in fluorescence lifetime *in vivo* tomography. Efficient separation of tissue autofluorescence from the iRFP in fluorescence lifetimes allows to obtain a high imaging sensitivity.

47. Wang LV, Hu S: **Photoacoustic tomography: in vivo imaging from organelles to organs**. *Science* 2012, **335**:1458-1462.

48. • Filonov GS, Krumholz A, Xia J *et al.*: **Deep-tissue photoacoustic tomography of a genetically encoded near-infrared fluorescent probe**. *Angew Chem Int Ed Engl* 2012, **51**:1448-1451.
The first application of a NIR FP in photoacoustic tomography. Photoacoustic imaging allows to obtain substantially better resolution in deep tissues than purely optical imaging methods and co-register signal from endogenous absorbers, such as hemoglobin.

49. Krumholz A, Shcherbakova DM, Xia J *et al.*: **Multicontrast photoacoustic in vivo imaging using near-infrared fluorescent proteins**. *Sci Rep* 2014, **4**:3939.

50. Tzoumas S, Nunes A, Deliolanis NC, Ntziachristos V: **Effects of multispectral excitation on the sensitivity of molecular optoacoustic imaging**. *J Biophotonics* 2014:9999.